Control of Self-Assembling Processes of Polyamidoamine Dendrimers and Pd Nanoparticles

Hirokazu Tanaka,[†,‡] Takeji Hashimoto,*[,†,‡] Satoshi Koizumi,*[,†] Hideaki Itoh,[‡] Kensuke Naka,[‡] and Yoshiki Chujo[‡]

Advanced Science Research Center (ASRC), Japan Atomic Energy Agency (JAEA), Tokai, Ibaraki 319-1195, Japan, and Department of Polymer Chemistry, Graduate School of Engineering, Kyoto University, Katsura, Kyoto 615-8510, Japan

Received September 8, 2007; Revised Manuscript Received December 12, 2007

ABSTRACT: We have investigated the self-assembly formed by palladium acetate ($Pd(OAc)_2$) and polyamidoamine dendrimers ($GN\text{-}NH_2$) in a mixed solvent of methanol and *N*,*N*-dimethylformamide. We aim to explore effects of the generation number (*GN*) and concentration of the dendrimers, [$GN\text{-}NH_2$], on the self-assembly of the dendrimers (defined hereafter as "templates") and the Pd nanoparticles inside the templates in order to clarify physical factors controlling the self-assembling mechanisms. For this purpose, we changed *GN* from 0 to 4 and [$GN\text{-}NH_2$] from 0.03 to 2.7 mM, keeping the concentration of $Pd(OAc)_2$, [$Pd(OAc)_2$], at a fixed value of 3.6 mM. The self-assemblies of the templates and the Pd nanoparticles were investigated by means of a combined method of small-angle neutron and X-ray scattering, ultra-small-angle X-ray scattering, dynamic light scattering, and transmission electron microscopy. We elucidated the following two facts concerning the effects of increasing *GN* on the self-assembly under a fixed value of [$-NH_2$] such that [$Pd(OAc)_2$]/[$-NH_2$] = 3.33, where [$-NH_2$] is molar concentration of the peripheral amine group of dendrimers having varying *GN*. (i) The size of the templates becomes smaller, while the number density of the templates increases. This trend is well explained from the viewpoint that the effective binding force between the templates via attractive interactions of $Pd(OAc)_2$ and amine groups of the dendrimers, which belong to different templates, becomes weak relatively to the random thermal force acting on the templates. (ii) The size of Pd nanoparticles becomes larger with increasing *GN*. This result can be rationalized by the following two effects: (a) increasing number fraction of $Pd(OAc)_2$ molecules, which are easily reduced to Pd(0) atoms; (b) increasing number density of $Pd(OAc)_2$ per single template as detailed in the text (section 4.2.1. and 4.2.3.). As for the effect of [$GN\text{-}NH_2$], we found that the templates are formed only when [$GN\text{-}NH_2$] falls below a critical value and thereby a sufficient amount of $Pd(OAc)_2$ exists as the binders between the dendrimers. Otherwise dendrimers are molecularly dispersed in solution.

1. Introduction

We have investigated the self-assembly of molecules in chemically reacting systems which are brought about by mixing the following two stable solutions of (a) and (b): (a) $Pd(OAc)_2$ in *N*,*N*-dimethylformamide (DMF) and (b) polyamidoamine (PAMAM) dendrimers ($GN\text{-}NH_2$) in methanol where *GN* designates generation number of the dendrimers. We previously found the following pieces of evidence for $G1\text{-}NH_2$ with a fixed concentration of $Pd(OAc)_2$ and $G1\text{-}NH_2$ ([$Pd(OAc)_2$] = 3.6 mM and [$G1\text{-}NH_2$] = 0.14 mM, respectively):[1,2] (1) the dendrimer molecules first self-assemble into spherical aggregates of ∼60 nm in diameter, mediated by attractive interactions between $Pd(OAc)_2$ and the amine groups in the dendrimers; (2) subsequently $Pd(OAc)_2$ are reduced to Pd(0) atoms, and the Pd(0) atoms further aggregate into Pd nanoparticles, both processes occuring within the self-assembled dendrimers as a "template" (see Figure 11 of ref 1). We found that in this reaction system $Pd(OAc)_2$ plays important roles as both the binders of the dendrimer aggregates and a source of the Pd nanoparticles. In this work, we aim to elucidate effects of (i) *GN* and (ii) concentration of the dendrimers, [$GN\text{-}NH_2$], upon the self-assembly. In more details, we shall explore a criterion for the dendrimers to exist in the solution as a stable dispersion of the aggregates (templates) or as a stable molecular dispersion. In the former case, we shall further explore how the size of the templates, R_{temp}, and Pd nanoparticles, R_{nano}, are affected by the two parameters.

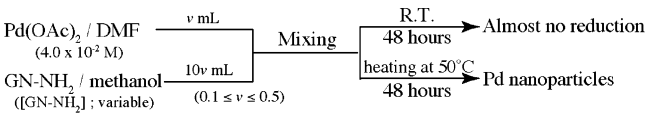

Figure 1. Experimental procedures to set up the chemically reacting systems which involves self-assembly of the dendrimers and chemical reduction of $Pd(OAc)_2$ into Pd nanoparticles.

So far there have been large numbers of studies on the synthesis of metal nanoparticles by using dendrimers as templates.[3−11] The originality or uniqueness of this study compared with the previous studies can be briefly summarized in the following three points: (i) large ratio of concentrations of metal ions and dendrimers, $Z = [M^{n+}]/[GN\text{-}X]$, where X designates the peripheral functional groups of dendrimers ($-NH_2$, in this study), (ii) nonaqueous solvent, and (iii) weak strength of reducing agents. These details were discussed in the previous work[1] and hence will not be repeated here.

2. Experimental Section

2.1. Sample Specimens. We prepared two stable solutions: (i) solution A, a transparent but dark red DMF solution of $Pd(OAc)_2$ (4.0×10^{-2} M) and (ii) solution B, a colorless and transparent methanol solution of $GN\text{-}NH_2$ with [$GN\text{-}NH_2$] varying from 3.0×10^{-2} to 3.0 mM and *GN* ranging from 0 to 4. The characteristics of the dendrimers used in this work are listed in Table 1. All the

* To whom correspondence should be addressed. E-mail: hashimoto.takeji@jaea.go.jp; koizumi.satoshi@jaea.go.jp.
† Japan Atomic Energy Agency (JAEA).
‡ Kyoto University.

10.1021/ma702034x CCC: $40.75
Published on Web 02/12/2008

Table 1. Characteristic Properties of PAMAM Dendrimers of Different Generations

generation number, *GN*	*FW* (g mol^{-1})	*X*(total N)[a]	*X*(−NH_2)[b]	*X*(−N−)[c]	*X*(amide)[d]	R_g (nm)[e]	density (g cm^{-3})
0	516.69	10	4	2	4	0.493	0.854
1	1429.88	26	8	6	12	0.746	0.820
2	3256	58	16	14	28	0.917	0.860
3	6909	122	32	30	60	1.12	0.863
4	14215	250	64	62	124	1.45	0.813

[a] The total number of N atoms per molecule. [b] The number of primary amine groups per molecule. [c] The number of tertiary amine groups per molecule. [d] The number of amide groups per molecule. [e] The values are reported in ref 12.

Table 2. Experimental Conditions Used in This Work

	Z[b]											
GN											$Z_{c,t,1}$[c]	$r_{c,t}$[c]
0	1.32	2.68	4.00	5.32	6.68						5.32	1.33
1	2.64	5.36	8.00	10.64	13.36	16.00	21.36 (#1)	26.64 (#2)	32.00 (#3)	42.64 (#4)	13.33	1.67
2	5.28	10.72	16.00	21.28	26.72	32.00		53.28 (#5)			26.67	1.33
3	10.56 (#6)	21.44 (#7)	32.00 (#8)	42.56 (#9)	53.44 (#10)	64.00 (#11)		106.56 (#12)			53.33	1.33
4	21.12	42.88	64.00	85.12							64.00	1.00
r[a]	0.33	0.67	1.00	1.33	1.67	2.00	2.67	3.33	4.00	5.33		

[a] $r \equiv [Pd(OAc)_2]/[-NH_2]$. [b] $Z \equiv [Pd(OAc)_2]/[GN\text{-}NH_2] = r \times 2^{GN+2}$ [c] Critical value above which the well-defined spherical template is formed. $[Pd(OAc)_2]$ was fixed at 3.6 mM for all the experimental systems to be treated in this work.

experimental systems employed in this study are listed in Table 2. They all contained a fixed $[Pd(OAc)_2] = 3.6$ mM as in the previous work.[1] The two solutions A and B were first mixed at room temperature (RT). The mixed solution was kept at RT or heated at 50 °C for 48 h for the reduction of $Pd(OAc)_2$, as shown in Figure 1.As clarified earlier,[1] methanol worked as a weak reducing agent at 50 °C, promoting the gradual reduction of $Pd(OAc)_2$ into Pd clusters. However, at RT, methanol did not work as a reducing agent, so only the template formation occurred, which is clarified later in section 4.4 (details in Supporting Information).

2.2. Small-Angle Neutron Scattering (SANS) Measurements. For a quantitative in situ structural analysis of the templates and the Pd nanoparticles in the reaction medium, SANS experiments were carried out in situ using the SANS-J spectrometer at the research reactor JRR-3 in JAEA (Japan Atomic Energy Agency), Tokai, Japan, as detailed elsewhere.[1] For further details, readers should refer to ref 1.

2.3. Small-Angle X-ray Scattering (SAXS) Measurements. The SAXS measurements were carried out at the SAXS beamline BL-15A in the Photon Factory of the High Energy Accelerator Research Organization, Japan. The SAXS profiles were obtained with a sample-to-detector length of 2300 mm covering q range of $0.1 < q < 2$ nm^{-1}. The scattering profiles were detected with a one-dimensional position sensitive proportional counter (PSPC). The wavelength of the incident X-ray was monochromatized to $\lambda = 0.1504$ nm. The SAXS profiles were corrected for the background scattering and the transmission. The absolute SAXS intensity in the unit of e^2/nm^3 was obtained by the standard nickel foil method.[13]

2.4. Combined SANS and SAXS Profiles. As elucidated previously,[1] at sufficiently small q's where q is the magnitude of scattering vector defined by

$$q = (4\pi/\lambda)\sin(\theta/2) \quad (1)$$

with λ and θ being wavelength of neutron beam and scattering angle, both SANS and SAXS depend on an average contrast difference between the template and the reaction medium. The absolute intensity of SANS was converted into the absolute intensity of SAXS in order to obtain a combined SANS and SAXS profiles in the absolute intensity scale of SAXS. Further details were already described in section 2.7 of ref 1 and will not be repeated here.

2.5. Ultra-SAXS (USAXS) Measurements. The USAXS measurements were performed with a Bonse Hart type USAXS apparatus[14,15] which consists of 18 kW rotating-anode X-ray generator (Bruker AXS K. K., Yokohama, Japan), grooved silicon crystals both for incident-beam monochromatization and for scattering-beam analyzer. The USAXS covered q range of $0.01 < q < 0.1$ nm^{-1}. The wavelength of the incident X-ray was 0.154 nm (Cu Kα line was used). The USAXS profiles were corrected for the background scattering, the transmission, the slit height, and the slit width smearings.

2.6. Dynamic Light Scattering (DLS) Measurements. DLS measurements were carried out on an ALV 5000 instrument (Langen, Germany) using Ar ion laser as the incident beam having a wavelength of 488 nm. The scattering angle was set at 90 and 135 °. A typical measurement time was 1800 s. The temperature of the sample was controlled at 25 °C within an error of ±0.1 °C.

2.7. Transmission Election Microscope (TEM) Observations. The self-assembly formed in the reaction medium was also investigated by a real-space method using TEM. The details are described in section 2.8 of ref 1 and hence will not be repeated here.

3. Results

3.1. Phase Diagram of This Reaction System. Let us first present the phase diagram of the system to be discussed in this work in the parameter space of $Z \equiv [Pd(OAc)_2]/[GN\text{-}NH_2]$ and *GN*. This phase diagram shown in Figure 2 was constructed by the following various methods: a visual observation of the system state (the data shown by unfilled circles), the combined SANS and SAXS method (the data shown by filled circles), the combined USAXS and SAXS method (the data shown by filled squares), and the DLS method (the data shown by filled tirangles). With the visual observation, we assessed a critical line $Z_{c,p}$, above which the templates and the Pd particles formed in the system grew into large agglomerates and precipitated, and a critical line $Z_{c,t,u}$, below which the templates and the Pd particles never precipitated. The gap between the two lines is uncertain due to either lack of the experimental data or difficulty in the visual determination.

For the sake of readers' convenience, we shall deliberately describe our conclusion here, though the detail will be described later in section 4.4. The critical lines $Z_{c,t,u}$ and $Z_{c,t,l}$ are the upper and lower bounds, respectively, for formation of well-defined stable aggregates with a smooth interface and a sharp interface

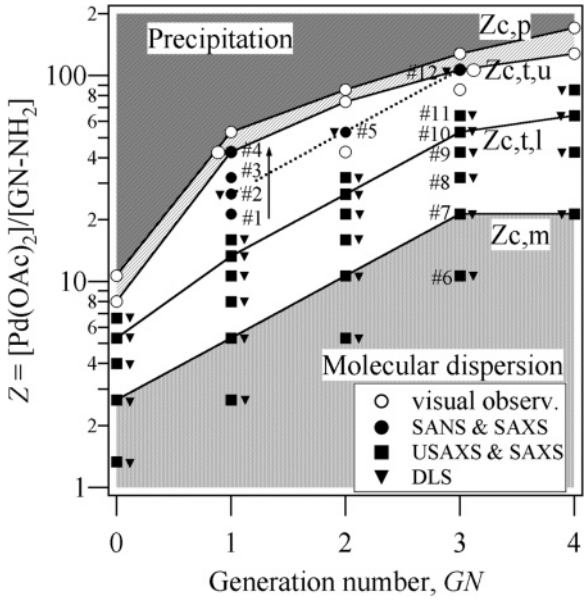

Figure 2. Phase diagram of the chemically reacting systems studied in this paper in the parameter space of *GN* and *Z* for a fixed value of $[Pd(OAc)_2] = 3.6$ mM.

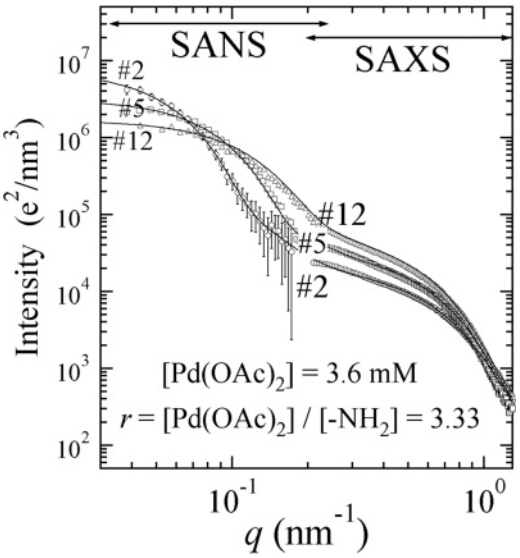

Figure 3. Combined SANS and SAXS profiles in the absolute intensity scale of SAXS (shown by symbols) for the mixed solutions of Pd-$(OAc)_2$/DMF and GN-NH_2/methanol, with *GN* varying from 1 to 3 under a fixed value of $r = [Pd(OAc)_2]/[-NH_2] = 3.3$ and $[Pd(OAc)_2] = 3.6$ mM. The solid lines represent the best-fitted theoretical results by using eqs 3−5.

boundary. $Z_{c,m}$ is the critical line below which the dendrimers are molecularly dispersed in the system. In the gap between the two lines, $Z_{c,t,l}$ and $Z_{c,m}$, the dendrimers do not form the stable aggregates as those above $Z_{c,t,l}$ but rather form kind of aggregates which dynamically fluctuate in their size and shape. The aggregates do not have a well-defined smooth interface and sharp interfacial boundary.

3.2. Generation Dependence of the Templates and the Pd Nanoparticles. We investigated effects of *GN* on both the templates and the Pd nanoparticles under a fixed value of $r = 3.33$ and $[Pd(OAc)_2] = 3.6$ mM. Here *r* is defined by $r \equiv [M^{n+}]/[-NH_2]$, with $[-NH_2]$ being the molar concentration of the peripheral amine groups of the dendrimers having varying *GN*. It should be noted that an increase of *GN* from 1 to 3 under these conditions involves an increase in the *Z* value or the change of the system state from #2 to #5 to #12 (see Table 2) along the dotted line in the phase diagram shown in Figure 2 in the region between the line $Z_{c,t,u}$ and the line $Z_{c,t,l}$. Note that *GN* and *Z* are interrelated under the fixed conditions of *r* and $[Pd(OAc)_2]$ as described above.

3.2.1. SAS (Small-Angle Scattering) Results. The templates and the Pd nanoparticles formed in the solutions were investigated by means of the SAS method (the combined SANS and SAXS measurements). Figure 3 shows the SAS profiles. Because the scattering vector *q* is related to the characteristic length in real space, ξ, by $q = 2\pi/\xi$, the scattering at lower and higher *q* regions is considered to arise dominantly from the templates and the Pd nanoparticles, respectively. At the first sight of these profiles, we can notice the following two obvious features regarding the generation dependence.

First, the SANS scattering profile at the lower *q* region of $q < 0.2$ nm^{-1} tends to shift as a whole toward a higher *q* region with increasing *GN* (a high *q* shift). Second, the SAXS scattered intensity at the higher *q* region of $q > 0.2$ nm^{-1} becomes larger and the profile as a whole tends to shift toward a smaller *q* region with increasing *GN* (a low *q* shift). These trends can be intuitively interpreted respectively as follows. With increasing *GN*, (i) the templates become smaller as evidenced by the observed high *q* shifts of the SANS profiles and (ii) the size of the Pd nanoparticles tends to become large, as implied from the increase in the scattered intensity and the low *q* shift found in the SAXS profiles. The detailed quantitative analysis of the scattering profiles will be discussed later in section 4.2.1.

3.2.2. TEM Observations. The same solutions used for SANS and SAXS measurements were investigated under TEM observation. The TEM images obtained from the solutions with $GN = 1$, 2, and 3 are shown in Figure 4 panels a, b, and c, respectively. In all TEM images, relatively small black dots correspond to Pd nanoparticles and relatively large gray domains, as marked by a circle, correspond to the templates. It is worth noting that almost all of the Pd nanoparticles seem to be entrapped in the templates regardless of *GN*. It is also noted that as *GN* increases the templates become smaller; the templates have an average diameter of ca. 70, 40, and 20 nm for $GN = 1$, 2, and 3, respectively. This trend is fully consistent with the SAS results described in section 3.2.1. We would like to point out here that in Figure 4b,c the templates appear to be linked together, forming a wormlike superstructure. However, we must note that such a superstructure may be formed during the solvent evaporation process of the specimens for TEM observations, because the process causes a change in template concentration and an aggregation of the templates driven by surface tension.[1,16,17] Therefore, just from the TEM image alone, we cannot conclude whether the wormlike superstructure of the templates really exists in the reaction solution or not. In order to clarify this point, it is necessary to carry out quantitative analysis of SAS observed in situ in the reaction solution (see section 4.2 for details).

With regard to the size of the Pd nanoparticles, it appears that the average size becomes slightly larger with increasing *GN*, which is also consistent qualitatively with the SAS results. Moreover, the number density of the Pd nanoparticles per template seems to decrease with increasing *GN*. This seems to be reasonable from the following viewpoints. (i) The total number of Pd atoms produced should be approximately the same for the three samples because of the constant value of $[Pd(OAc)_2]$ (see the last paragraph of section 4.2.3 for details) and (ii) the number of the templates increases with *GN*, as will be clarified later in section 4.2.

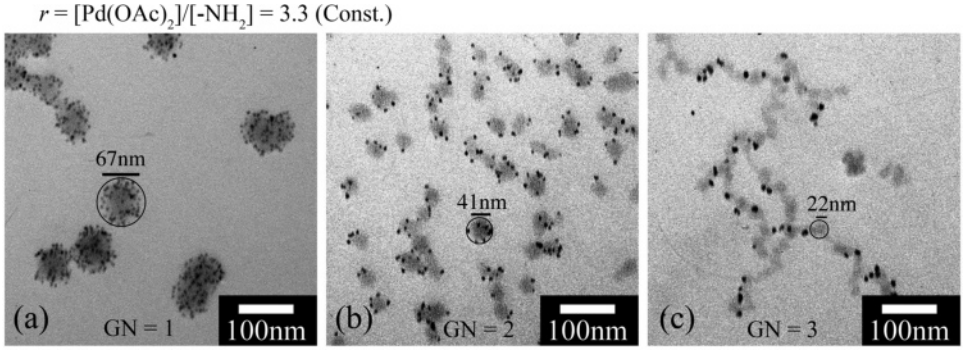

Figure 4. TEM images for the templates and Pd nanoparticles for the same specimens used in the SANS and SAXS experiments shown in Figure 4: (a) $GN = 1$, $Z = 26.4$ (#2), (b) $GN = 2$, $Z = 52.8$ (#5), and (c) $GN = 3$, $Z = 105.6$ (#12).

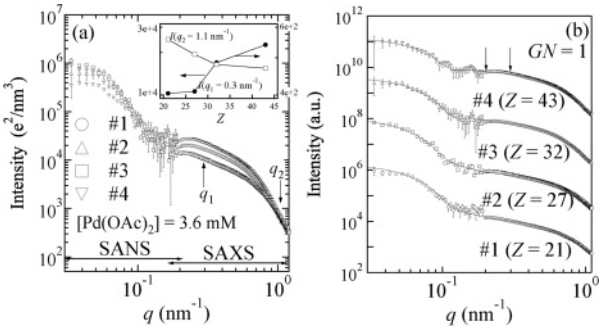

Figure 5. Combined SANS and SAXS profiles for the mixed solutions of $Pd(OAc)_2$/DMF and G1-NH_2/methanol with Z varying from 21 (#1) to 43 (#4).

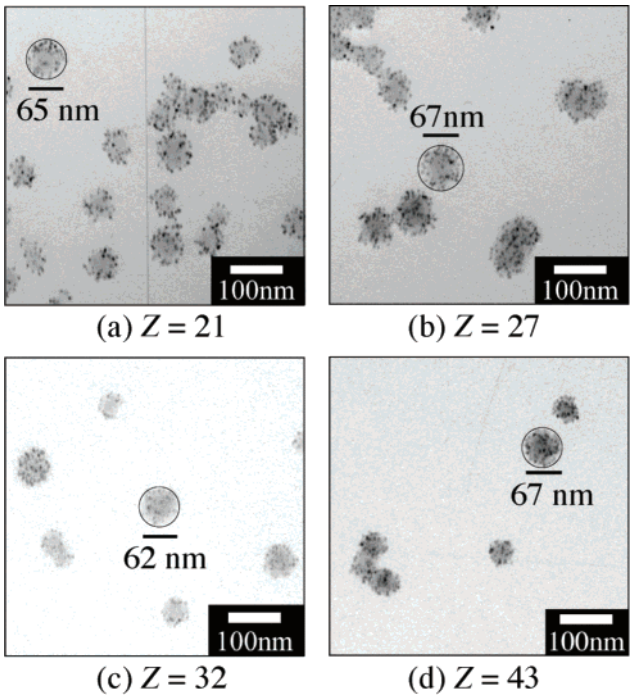

Figure 6. TEM images for the templates and Pd nanoparticles for the same specimens used in the SANS and SAXS experiments shown in Figure 5. Z changed from 21 (part a) to 43 (part d) for a fixed value of $GN = 1$.

3.3. Effect of Changing *Z* Values on the Templates and the Pd Nanoparticles. For this purpose, we prepared four representative solutions using G1-NH_2 with Z ranging from 21 to 43 (#1 to #4 in Table 2), satisfying again the conditions of $Z_{c,t,l} < Z < Z_{c,t,u}$ (marked by the arrow in Figure 2).

Table 3. Summary of Experimental Results of *GN* Dependence on R_{nano} and R_{temp} for $r = 3.3$

GN	R_{temp} (nm)	σ_{temp}/R_{temp}	R_H (nm)[a]	N_{temp}[b]	R_{nano} (nm)	σ_{nano}/R_{nano}	ϕ_n[b,c]
1	31	0.30	30	1	1.8	0.55	1
2	19	0.28	21	4.1	2.4	0.40	0.19
3	11	0.40	18	21.4	2.8	0.32	0.028

[a] Evaluated from DLS. [b] Relative values. [c] The volume fraction of the nanoparticles in the templates as evaluated from SANS.

3.3.1. SAS Results. Figure 5a shows the SAS profiles for the four solutions. It is found that at the lower q regions of $q < 0.2$ nm^{-1} covered by SANS, the profiles appear to be roughly identical to each other. This implies that once Z exceeds the critical value $Z_{c,t,l}$ the template size and shape hardly change with increasing Z. On the contrary, at the higher q regions of $q > 0.2$ nm^{-1} covered by SAXS, the scattered intensity constantly increases and the profiles tend to show a low q shift with Z. This trend is also clarified by the intensity at the particular q values of q_1 and q_2, shown by the arrows as a function of Z (see the inset). This trend implies that the size of the Pd nanoparticles increases with Z.

3.3.2. TEM Observations. Figure 6a−d show the TEM images obtained for the four solutions used in the SANS and SAXS measurements. We can clearly find that even though Z values increase from 21 to 43 almost no change is observed for the size of the templates, with its size being ca. 60−70 nm. In addition, we can find the number density of the templates tends to decrease with Z, which is well predictable from the following two facts: with increasing Z, [G1-NH_2] decreases (because [Pd-$(OAc)_2$] is fixed) but the size of the templates is unchanged. Thus, it is also confirmed from TEM observations that once the template structures are formed ($Z > Z_{c,t,l}$) their size does not change much with Z (the average diameter is around 60−70 nm). It seems to be difficult to quantitatively investigate how the size of Pd nanoparticles is affected by Z from the TEM images.

4. Analysis and Discussion

4.1. Static SAS Function Used in This Work. We derived a general scattering function, $I(q)$, for a single template which contains the Pd nanoparticles as its internal structures[2]

$$I(q) = (\text{const})V_{temp}\rho_0^2\left[S_{temp}(q) + \frac{\langle\eta^2\rangle}{\rho_0^2}S_{temp}(q) * S_{nano}(q)\right] \quad (2)$$

where V_{temp} is the volume of the template. The average contrast, ρ_0, of the template containing nanoparticles is given by $\rho_0 = \phi_n\rho_n + (1 - \phi_n)\rho_t$, where ρ_n and ρ_t are scattering contrasts of

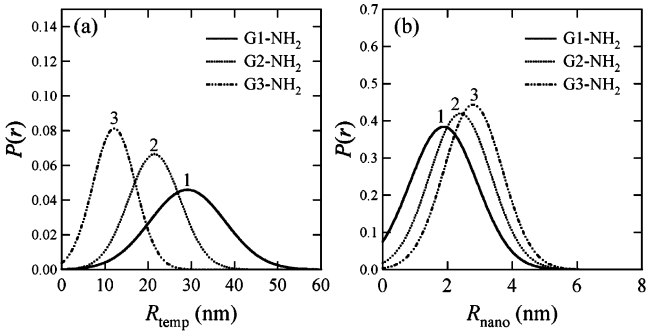

Figure 7. *GN* dependence of (a) the size distribution function $P(r)$ for the templates and (b) $P(r)$ for the Pd nanoparticles calculated from the best fit of the combined SAS profiles shown in Figure 3 with the theoretical scattering functions.

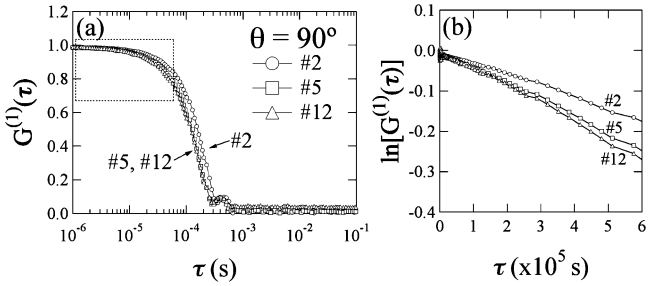

Figure 8. (a) Time correlation function for the systems having varying *GN* (*GN* = 1 (#2), 2 (#5), and 3 (#12)) with a fixed value of $r = [Pd(OAc)_2]/[-NH_2] = 3.3$. (b) Initial decay in $G^{(1)}(\tau)$ as demonstrated by ln $G^{(1)}(\tau)$ vs τ for the data encompassed by the broken square in part a.

the nanoparticles and the templates, respectively, and ϕ_n is the volume fraction of nanoparticles inside the template. $<\eta^2>$ stands for mean-squared spatial contrast fluctuations within the template, $\eta(r)$. In the case when $S_{temp}(q)$ (the scattering function for a homogeneous template) is described by a sphere of radius, R_{temp} $S_{nano}(q)$ (the scattering arising from a spatial distribution of nanoparticles inside the template) is described by an independent scattering from the total number, N_{nano}, of spherical nanoparticles having the radius, R_{nano}, and there are size distributions for R_{temp} and R_{nano}, the average scattering function $<I(q)>$ is given by

$$\langle I(q)\rangle = (\text{const})\rho_0^2\left\{\langle V_{temp}^2\Phi^2(qR_{temp})\rangle + \phi_n\frac{(\rho_n-\rho_t)^2}{\rho_0^2}\langle[V_{nano}^2\Phi^2(qR_{nano})]\rangle * \langle[V_{temp}^2\Phi^2(qR_{temp})]\rangle\right\} \quad (3)$$

where $\langle V_J^2\Phi^2(qR_J)\rangle$ means the average of $V_J^2\Phi^2(qR_J)$ with respect to a normalized distribution function $P_J(R)$ for the radius R (J = temp or nano). We assume that $P_J(R)$ is given by the Gaussian distribution with average radius R_J and standard deviation of σ_J

$$P_J(R) = \frac{1}{\sqrt{2\pi}\sigma_J}\exp\left[-\frac{(R-R_J)^2}{2\sigma_J^2}\right], \int_0^\infty P_J(R)\,dR = 1 \quad (4)$$

where V_J (J = temp or nano) denote the volume of the templates or nanoparticles, respectively. $\Phi^2(qR)$ denotes the form factor of a sphere given by

$$\Phi(qR) = 3[\sin(qR) - (qR)\cos(qR)]/(qR)^3 \quad (5)$$

In the case when $R_{temp} \gg R_{nano}$, eq 2 is much simplified.[2] However, in this work, we used eq 2 since R_{nano}/R_{temp} increases up to about 0.16 as *GN* increases (see Table 3). Validity of the assumption for isolated templates and independent scattering from nanoparticles was well confirmed by means of the analysis previously discussed in section 4 in ref 2.

4.2. *GN* Dependence of R_{temp} and R_{nano}. 4.2.1. SAS Analysis. Panels a and b of Figure 7 respectively show the normalized size distribution functions $P_{temp}(R)$ and $P_{nano}(R)$ for the templates and the Pd nanoparticles as evaluated by the best fit of the experimental SAS profiles with the theoretical profiles calculated using eqs 3−5, as shown in Figure 3 where the best fitted theoretical results are shown by the solid lines. We find that the theoretical scattering functions quite well reproduce the measured scattering profiles. The evaluated R_{temp}'s and R_{nano}'s are also listed in Table 3 together with the evaluated relative values of N_{temp}'s and ϕ_n's, where N_{temp} denotes the number density of the templates in the reaction solution. The relative values of N_{temp}'s and ϕ_n 's can be evaluated from the curve fitting using eq 3, because the front factor of the bracket $< >$ in the first term of right-hand side of eq 3, K_{first}, is proportional to N_{temp} while that of the second term, K_{second}, is proportional to N_{temp} and ϕ_n

$$K_{first} \propto N_{temp}\rho_0^2 \quad (6)$$

$$K_{second} \propto N_{temp}\phi_n(\rho_n - \rho_t)^2 \propto N_{temp}\phi_n \quad (7)$$

The values R_H in Table 3 will be discussed later in section 4.2.2.

As clearly shown in Figure 7a and Table 3, the average template size R_{temp} decreases with *GN* while the relative standard deviation σ_{temp}/R_{temp} tends to increase with *GN*. It is also clear that the average size of the Pd nanoparticles R_{nano} increases but its relative standard deviation decreases with increasing *GN* as evidenced in Figure 7b and Table 3. Moreover, it is noted that the evaluated R_{temp} and R_{nano} from SAS are well consistent with those estimated from the TEM images in Figures 4a−c.

4.2.2. DLS Analysis. As an alternative method for investigating the effect of changing *GN* on R_{temp}, we have conducted the DLS measurements. Figure 8a shows the time correlation function, $G^{(1)}(\tau)$, for the same three solutions as those described in section 3.2.1. $G^{(1)}(\tau)$ is related to translational and/or cooperative motions of the templates in the solutions.[20] Figure 8b highlights a part of $G^{(1)}(\tau)$ encompassed by the square marked by broken line at a small τ region in Figure 8a.

As *GN* increases, the slope of ln $G^{(1)}(\tau)$ vs τ obviously becomes steeper, indicating a faster decay in concentration fluctuations in the solution. The slope (initial decay rate), $\Gamma(q)$, can be expressed by $\Gamma(q) = Dq^2$ where D denotes translational diffusion coefficient of the templates in the reaction medium. According to the Einstein−Stokes law, D is related to the hydrodynamic radius of the templates, R_H

$$R_H = k_B T/(6\pi\eta D) \quad (8)$$

where k_B is the Boltzmann's constant, T is the absolute temperature, and η is the viscosity of the reaction medium. Thus, one can evaluate R_H for the templates in the solutions from the value of $\Gamma(q)$. The obtained R_H values, which are also listed in Table 3, are well consistent with the values independently estimated from SAS except for *GN* = 3. The discrepancy found for *GN* = 3 with respect to $R_{temp} < R_H$ may infer a temporal association of spherical templates in the short timescale covered by the DLS experiments, although spherical templates may be

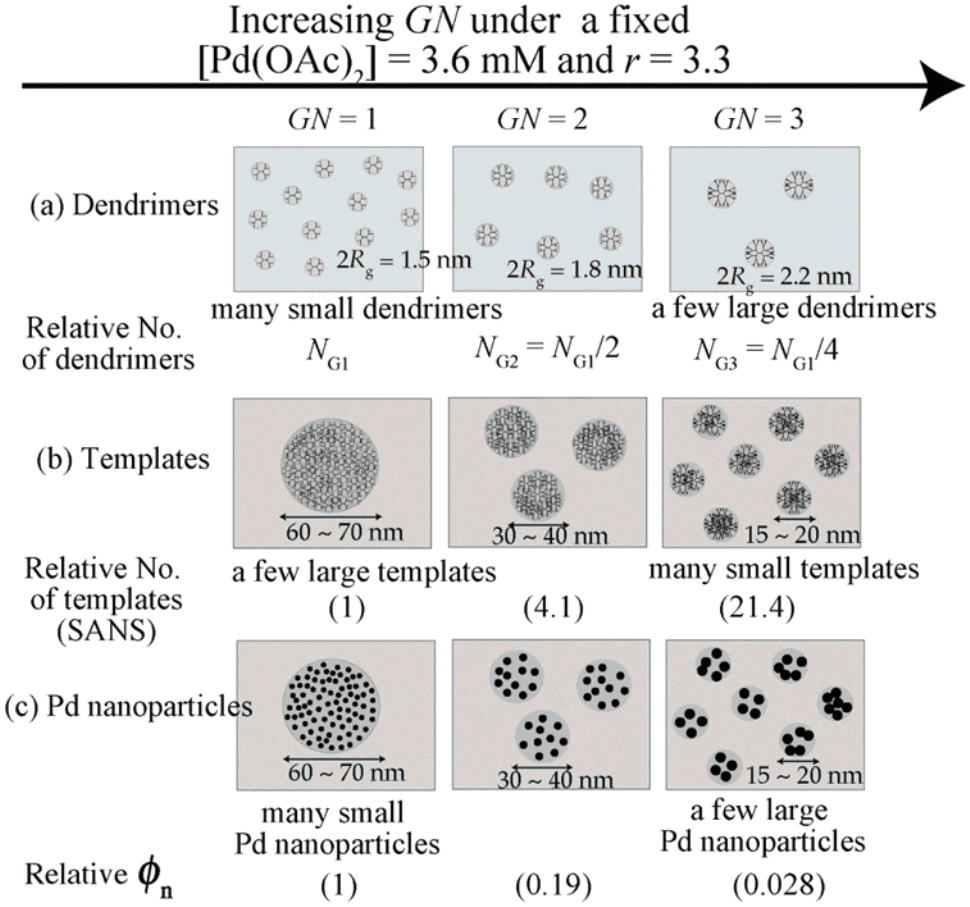

Figure 9. Schematic illustrations of effects of changing *GN* upon the dendrimers (a), the templates (b), and the Pd nanoparticles (c) under a fixed value of $r = [Pd(OAc)_2]/[-NH_2] = 3.3$ and $[Pd(OAc)_2] = 3.6$ mM.

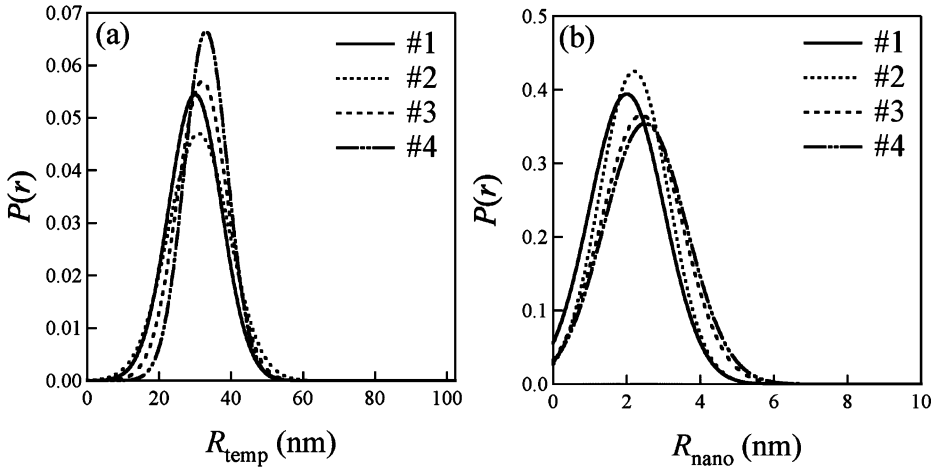

Figure 10. *Z* dependence of the size distribution function $P(r)$ (a) for the templates and (b) for the Pd nanoparticles calculated from the best fit of the combined SAS profiles with the theoretical scattering functions shown in Figure 5.

Table 4. Summary of Experimental Results on *Z* Dependence of R_{nano}, R_{temp}, and So Forth

Z	R_{temp} (nm)	σ_{temp}/R_{temp}	N_{temp}[b]	R_{nano} (nm)	σ_{nano}/R_{nano}	ϕ_n[b]
21	30	0.24	1	2.0	0.51	1.0
27	31	0.27	0.7	2.2	0.43	1.2
32	32	0.22	0.58	2.4	0.45	1.3
43	33	0.18	0.29	2.5	0.45	2.3

[a] All values in the table are evaluated from curve fitting of the SAS profiles. [b] Relative values.

isolated on a statistical average over the long timescale covered by SANS experiments. Therefore the SANS and DLS results imply that the wormlike structures of the templates shown in Figure 4 do not exist stably in the solution over the long timescale (0.5−1 h), as observed by SANS. This implication is reasonable from a viewpoint of the very low concentration of the templates (about 0.015% in volume fraction for any *GN*).

4.2.3. Discussion. Let us now discuss the effects of increasing *GN* under the fixed conditions specified in section 3.2 on self-assembly of templates and the Pd nanoparticles. We postulate that R_{temp} is controlled by a balance of the two opposing physical factors of entropic and energetic origin. One is the random thermal force acting on the dendrimer molecules themselves,

which tends to force the dendrimer molecules to be molecularly dissolved in space, thereby gaining entropy. The other one is the energetic factor associated with attractive interactions of Pd(OAc)$_2$ with the amine groups of the dendrimers. These attractive interactions between the amine groups belonging to different dendrimers and Pd(OAc)$_2$ tend to form the templates, in which Pd(OAc)$_2$ act as a binder or physical cross-linker between dendrimers. The balance of the opposing physical factors should stabilize the dispersion of the templates of given sizes in the solution.

As *GN* increases, the total number of amine groups per dendrimer (including the peripheral amine groups) increases. This favors the interdendrimer associations and hence the template formation in one hand. On the other hand upon increasing *GN*, the conformation freedom (or flexibility) of denderimers decreases and thereby dendrimers become more rigid. This disfavors the template formation because of increasingly severe steric hindrance for the interdendrimer cross-linking or because of increasing deformation of dendrimer conformations involved by a given amount of interdendrimer cross-linking.[21] Consequently, a number fraction of amines effective for interdendrimer cross-linking decreases with increasing *GN*, which makes the effective attractive force between the dendrimers and/or templates relatively weak compared to the random thermal force. This will explain why R_{temp} decreases with *GN*.

The effects of *GN* on the templates and the nanoparticles are summarized in Figure 9. As *GN* increases from 1 to 3, the relative [GN-NH$_2$] decreases in ratio to 1:0.5:0.25, respectively, under the fixed values of r and [Pd(OAc)$_2$] (see Table 1), because the number of primary amine groups increases in proportion to 1:2:4, respectively. As a consequence, a fewer but larger dendrimers exist in the system as schematically shown in Figure 9a. The SANS results on R_{temp} an N_{temp} (see Table 3) revealed that a larger number of smaller templates is stabilized with increasing *GN* as schematically shown in Figure 9b, which was predicted to be reasonable on the basis of qualitative discussion given in the above paragraph. The number density of the templates, N_{temp}, estimated from the SANS (see Table 3) seems to be reasonable from the following experimental point of view also. The total volume of the dendrimers in the system can be calculated both from the SANS data of R_{temp} and N_{temp} ($V_{t,SANS} \propto N_{temp} R_{temp}^3$) and from the stoichiometric data ($V_{t,stoich} \propto N_{GN} R_{g,GN}^3$ where N_{GN} and R_{GN} (Table 1) are the number and radius of gyration of GN-NH$_2$. The volume ratio of G1-NH$_2$:G2-NH$_2$:G3-NH$_2$ is 1:0.929:0.846 on the basis of the stoichiometric data, while it is 1:0.944:0.856 on the basis of the SANS data. The two results are found to be in good agreement.

We shall now discuss the effects of *GN* on R_{nano} (Table 3 and Figure 7b). We estimate the average number density of Pd(OAc)$_2$ in the templates, $\rho_{Pd/temp,GN}$, for GN-NH$_2$. This is given by

$$\rho_{Pd/temp,GN} \propto [N_{temp,GN} R_{temp,GN}^3]^{-1} \quad (9)$$

because of the constant value for [Pd(OAc)$_2$], where the subscript *GN* in $N_{temp,GN}$ and $R_{temp,GN}$ denotes the respective quantities for GN-NH$_2$. These quantities were estimated from the respective values shown in Table 3. The relative ratio of $\rho_{Pd/temp,GN}$ is 1:1.06:1.16. Thus, the local concentration of Pd(OAc)$_2$ in a given template increases with *GN*. This fact, together with another fact that the fraction of the reducible Pd(OAc)$_2$ increases with *GN* (see Table 1) for the reason described immediately below, would explain the increase in R_{nano} with *GN*, as schematically illustrated in Figure 9c. In Table 1, we should note the following two points. (i) With increasing *GN*, the number fraction of the primary amine groups among other functional groups like the tertiary amine groups and the amide groups, which strongly interacts with Pd(OAc)$_2$, decreases; (ii) The Pd(OAc)$_2$ interacting with the primary amine groups is likely to be nonreducible with methanol. These two points imply that the number of reducible Pd(OAc)$_2$ molecules and therefore Pd atoms formed will increase with increasing *GN* under the fixed value of [Pd(OAc)$_2$] = 3.6 mM.

4.3. *Z* Dependence of R_{temp} and R_{nano}. Let us now discuss the effects of changing Z with R_{temp} on R_{nano} for G1-NH$_2$ (see Figures 5, 6, 10, and Table 4). This change of Z results in a decreasing number of G1-NH$_2$, as will be schematically shown later in Figure 11a, and corresponds to the change of the system state from #1 to #4 (Table 2) along the arrow marked in the phase diagram shown in Figure 2 in between the lines $Z_{c,t,l}$ and $Z_{c,t,u}$.

4.3.1. SAS Analysis. Parts a and b in Figure 10 show respectively the size distribution functions of the templates and the Pd nanoparticles evaluated from the best fit of the experimental SAS profiles (shown by symbols) with theoretical one as shown in Figure 5b. The best-fitted theoretical profiles are shown by the solid lines in Figure 5b.[22] The obtained parameters R_{temp}, σ_{temp}, R_{nano}, and σ_{nano} are listed in Table 4. The results show almost no Z dependence on R_{temp} ($R_{temp} \cong$ 32.5 nm), implying that the size of the templates hardly changes with Z once Z exceeds $Z_{c,t,l}$. However, R_{nano} tends to increase systematically from 2.0 to 2.5 nm with increasing Z values.

4.3.2. Discussion As briefly noted in section 3.3 in conjunction with the TEM images in Figure 6, once Z exceeds $Z_{c,t,l}$, it hardly affects R_{temp}. Actually, the theoretical analysis of SANS profiles yielded roughly the same value of R_{temp} for all the Z values as shown in Table 4. The trend is schematically illustrated in Figure 11b. N_{temp} evaluated from the best-fit tends to decrease with increasing Z as seen in Table 4 and as described in the legend in Figure 11b. The trend is reasonable, because the total number of the dendrimers decreases with increasing Z, but R_{temp} is roughly independent of Z.[23] R_{nano} increases with increasing Z as shown in Table 4. This is interpreted as follows. The fact that R_{temp} is nearly independent of Z but N_{temp} decreases with Z implies that the number of Pd(OAc)$_2$ molecules, which binds the dendrimers together and that is not reduced to Pd(0) atoms, decreases with Z. Hence, the number of reduced Pd(0) atoms increases with Z, which in turn causes the increase of R_{nano}. This trend is schematically illustrated in Figure 11c.

4.4. SAS and DLS Analyses of Phase Diagram. Let us now explain how we determined the critical lines $Z_{c,t,u}$, $Z_{c,t,l}$, and $Z_{c,m}$ in the phase diagram shown earlier in Figure 2. The critical lines $Z_{c,t,l}$ and $Z_{c,m}$ were determined by using both the combined USAXS and SAXS methods at 27 data points which are shown by filled squares and DLS at 30 data points which are shown by filled triangles, while the critical line $Z_{c,t,u,}$ was determined by using the combined SANS and SAXS methods at 6 data points which are shown by filled circles. These measurements were carried out at 25 °C, at which Pd(OAc)$_2$ remains unreduced. Nevertheless, the dendrimer aggregates formed at 25 °C had almost the same size of those formed at 50 °C where Pd(OAc)$_2$ was reduced and thereby Pd nanoparticles were formed within the dendrimer aggregates (details in Supporting Information).

Among the many SAS and DLS results obtained in the parameter space of *GN* and Z, we present only a few typical data showing the effects of Z on the behavior of G3 dendrimer in Figure 12. The effects of Z on SAS and DLS behavior for

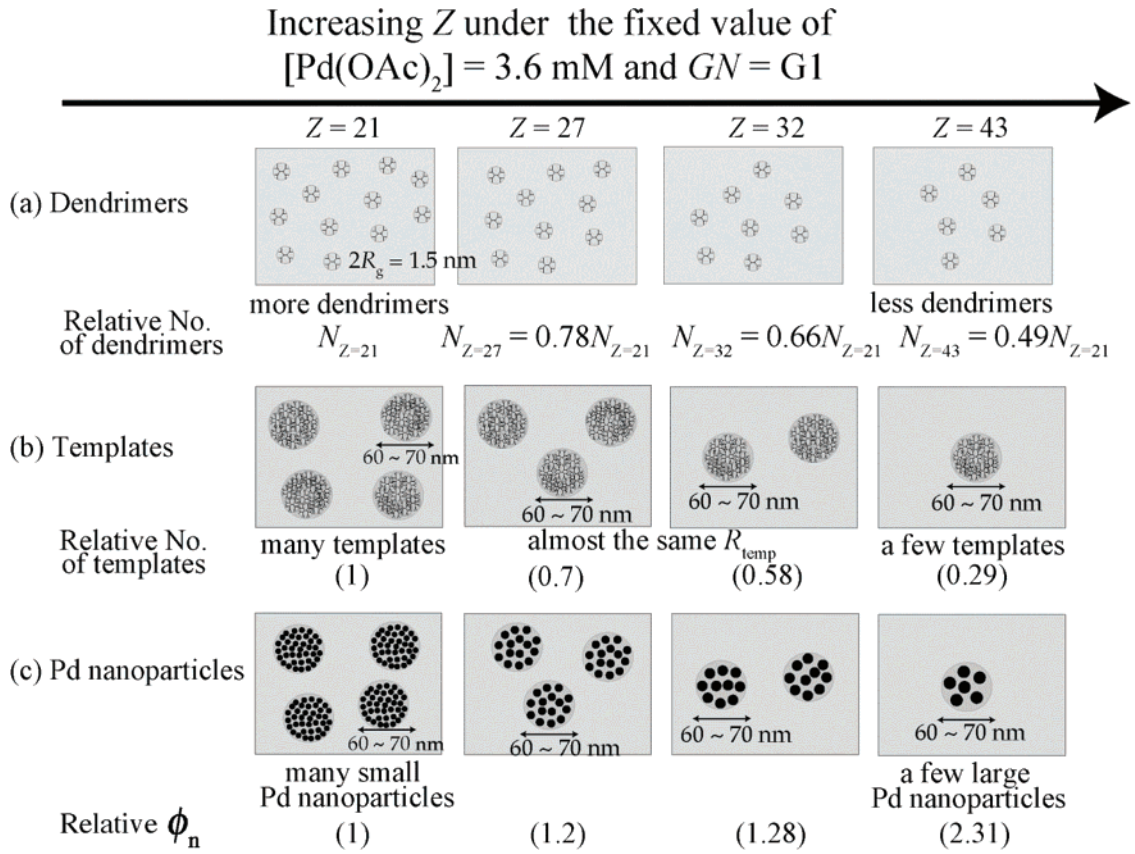

Figure 11. Schematic illustrations of effects of changing Z value on the dendrimers (a), the templates (b), and the Pd nanoparticles (c) under the fixed values of $[Pd(OAc)_2] = 3.6$ mM and $GN = 1$.

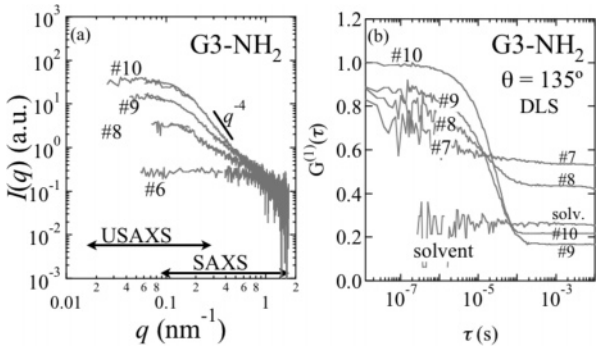

Figure 12. Z dependence of (a) the combined USAXS and SAXS profiles and (b) the time correlation functions for the solutions with $GN = 3$, Z varying from 10.6 to 53.4 (see Table 2 for the number attached to each curve).

dendrimers with other generations G0−G2 and G4 are similar to those shown in Figure 12, as will be detailed elsewhere.[24] Figure 12a presents the combined SAS (USAXS and SAXS) profiles for specimens #6 to #10 with Z values ranging from 10.6 to 53.4 (see Table 2). We found that the profiles #6 ($Z =$ 10.6) and #7 ($Z = 21.4$) exhibit the weakly q−dependent scattering profile, though only profile #6 is presented as a representative profile. The decrease of $I(q)$ at $q > 0.6$ nm^{-1} in this case is consistent with the independent scattering (the form factor) from isolated G3-NH_2's as reported by Prosa et al.[25] Thus the dendrimers are found to be molecularly dispersed in the system. This trend is illustrated in Figure 13a.

On the other hand, once Z becomes larger than the critical value $Z_{c,m}$, the excess scattering at the low q range of $q < 0.4$ nm^{-1} starts to appear remarkably, as demonstrated by the profiles #8 ($Z = 32$) and #9 ($Z = 42.6$). The profiles #10 ($Z =$ 53.4) and #11 ($Z = 64.0$) tend to show the power law behavior of q^{-4} at the high q region, though only the profile #10 is shown in the figure as a representative one. The results of #10 and #11 indicate the formation of well-defined templates having a smooth interface with a sharp interfacial boundary.[26] This trend is illustrated in Figure 13c.

Based upon the results discussed above, we can schematically illustrate a model for Z dependence of the templates as shown in Figure 13a−d, in which $Z_{c,m}$, $Z_{c,t,l}$, and $Z_{c,t,u}$ vary with GN as shown in Figure 2. It should be noted that the profiles #8 and #9 definitely show the scattering excess to the form factor for the isolated dendrimers themselves, indicating formation of aggregates of dendrimers. However, the aggregates do not appear to have a smooth interface with a sharp interfacial boundary as in the case of profiles #10 and #11. Therefore, for Z values between $Z_{c,m}$ and $Z_{c,t,l}$, the system forms a structure intermediate between that shown in part a and part c in Figure 13 and thereby some aggregates of dendrimers which are not well defined compared with those shown in part c.

We investigated the formation of the template structure also by DLS experiments. Figure 12b demonstrates typical DLS results for G3-NH_2. For $Z = 10.6$ (#6), $G^{(1)}(\tau)$ showed no apparent relaxation curve in the τ range covered in this study; $G^{(1)}(\tau)$ is almost identical to that for the solvent (methanol/DMF, 10/1, v/v). Hence, the dendrimer molecules themselves are expected to undergo cooperative diffusion in the timescale much shorter than that covered in this experiment. On the other hand, when $Z \geq 21.4$, $G^{(1)}(\tau)$ clearly showed relaxation in the timescale ranging from $\tau = 10^{-8}$ to 10^{-3} s, as shown by the correlation functions #7 to #10. We can find two kinds of correlation functions in this Z range. The correlation functions

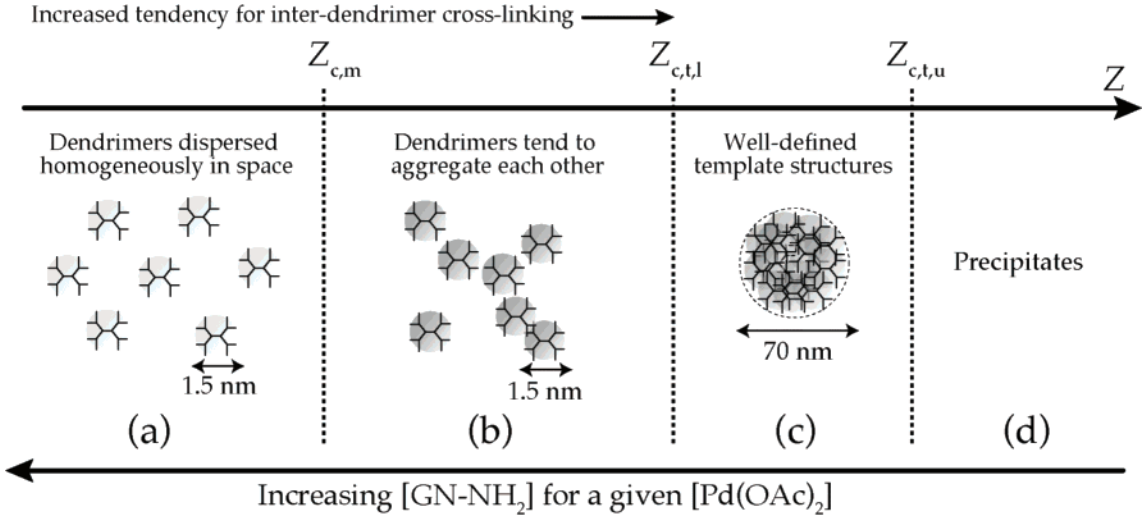

Figure 13. Schematic illustrations of the effect of changing *Z* values upon the template structures.

for $Z = 53.4$ (#10) and 64.0 (#11) were almost identical so that only the correlation function for $Z = 53.4$ is shown in Figure 12b. It exhibits essentially a single-exponential relaxation behavior in the timescale covered in this experiment; the relaxation curve indicates formation of well-defined aggregates (the templates) having a hydrodynamic radius of $R_H = 30$ nm, consistent with the values of R_{temp} measured by SANS, hence supporting the model shown in Figure 13c.

On the contrary, the correlation functions #7 to #9 exhibited a nonexponential relaxation behavior, which may indicate that the dendrimers form some sort of dynamical aggregates (e.g., worm-like mass-fractal structure), as schematically shown in Figure 13b. The fact that there are two kinds of relaxation behaviors depending on *Z* values was also found for other *GN*'s.[24] Thus we could evaluate the critical values $Z_{c,t,l}$ and $Z_{c,m}$ also by examining $G^{(1)}(\tau)$ as a function of *GN* and *Z*. The estimated values by DLS are exactly the same as those determined by the USAXS and SAXS. The estimated $Z_{c,t,l}$ (or $r_{c,t}$) values are summarized in Table 2 and shown in Figure 2.

Here it should be noted that the condition of $Z \cong Z_{c,t,l}$ corresponds to the critical value of *r*, $r_{c,t}$, which is approximately 1.33 on average as shown in Table 2. Thus, in the case of $Z \leq Z_{c,t,l}$ or $r \leq r_{c,t}$, the number of $Pd(OAc)_2$ molecules will be slightly less than that of the primary amine groups of the dendrimer. This will cause the situation where attractive interactions between the dendrimers and $Pd(OAc)_2$ molecules become weaker than the random thermal force on the dendrimers. Consequently, it is possible that dendrimers may be bound to the dynamically heterogeneous structures whose size and shape may change with time. In this *Z* regime, the associations may not show a perfect spherical shape with the well-defined interface.

5. Conclusion

We have studied the self-assembly of the system comprising $Pd(OAc)_2$ and PAMAM dendrimers in the mixed solvent system of methanol and DMF by means of the combined small-angle scattering technique. We elucidated that the self-assembly can be controlled simply by changing the generation number of the dendrimers *GN* and the concentration of the dendrimers [GN-NH_2]. With increasing *GN* under a fixed value of [$Pd(OAc)_2$] = 3.6 mM and a fixed value of $r = [Pd(OAc)_2]/[-NH_2] = 3.3$, we could obtain a smaller self-assembly (template) which encapsulates larger Pd nanoparticles (Figure 9c). We have also elucidated that the concentration of dendrimers strongly affects the self-assembly (Figure 13). If [GN-NH_2] is too large relative to [$Pd(OAc)_2$] (or $Z < Z_{c,m}$), the self-assembly cannot be formed and the dendrimers get dissolved homogeneously in the solution, as the earlier works reported,[3−11] even for the nonaqueous system studied in this work (Figure 13a). We found that there is a critical concentration of dendrimers for the formation of well-defined spherical self-assembly (Figure 13c), $Z_{c,t,l} = [Pd(OAc)_2]/[GN\text{-}NH_2]_{c,t,l}$. The critical concentration is found to be closely related to the critical value of $r = [Pd(OAc)_2]/[-NH_2]$, $r_{c,t}$, which is equal to about 1.33: Regardless of *GN*, once *r* exceeds $r_{c,t}$, the spherical self-assembly starts to grow (Table 2). We discovered the existence of intermediate heterogeneous self-assembly in the case of $Z_{c,m} < Z < Z_{c,t,l}$, as described in section 4.4 in conjunction with Figure 13b.

It may be possible that if some kinds of external fields such as electric fields, magnetic fields, and shear flow are imposed on the intermediate structures the structures may be easily affected by the fields. The effects of external fields are expected to be effective even for the self-assembly under the criterion of $Z > Z_{c,t,l}$ (Figure 13c) where the fields can be applied during or after the self-assembling process. Thus the results presented in this study may lead to a further precise control of the self-assembly of the system containing metal nanoparticles and dendrimers.

Acknowledgment. SAXS measurements were conducted under approval of the Photon Factory Advisory Committee (Proposal No. 15A/2004G266). The authors gratefully acknowledge Prof. M. Takenaka at Department of Polymer Chemistry, Kyoto University for his support on DLS measurements and useful comments on the DLS results and Dr. A. Chiba at Department of Physics, Keio University for her assistance on the synchrotron SAXS measurements.

Supporting Information Available: Details on the effect of temperature on the template structures by the combined SANS and SAXS method. This material is available free of charge via the Internet at http://pubs.acs.org.

References and Notes

(1) Tanaka, H.; Koizumi, S.; Hashimoto, T.; Satoh, M.; Itoh, H.; Naka, K.; Chujo, Y. *Macromolecules* **2007**, *40*, 4327−4337.
(2) Hashimoto, T.; Tanaka, H.; Koizumi, S.; Naka, K.; Chujo, Y. *J. Appl. Crystallogr.* **2007**, *40*, s73−s77.
(3) Zhao, M.; Sun, L.; Crooks, R. M. *J. Am. Chem. Soc.* **1998**, *120*, 4877−4878.

(4) Balogh, L.; Tomalia, D. A. *J. Am. Chem. Soc*. **1998**, *120*, 7355−7356.
(5) Esumi, K.; Suzuki, A.; Aihara, N.; Usui, K.; Torigoe, K. *Langmuir* **1998**, *14*, 3157−3159.
(6) Chechik, V.; Zhao, M.; Crooks, R. M. *J. Am. Chem. Soc*. **1999**, *121*, 4910−4911.
(7) Garcia, M. E.; Baker, L. A.; Crooks, R. M. *Anal. Chem*. **1999**, *71*, 256−258.
(8) Gröhn, F.; Bauer, B. J.; Akpalu, Y. A.; Jackson, C. L.; Amis, E. J. *Macromolecules*, **2000**, *33*, 6042−6050.
(9) Niu, Y.; Yeung, L. K.; Crooks, R. M. *J. Am. Chem. Soc*. **2001**, *123*, 6840−6846.
(10) Crooks, R. M.; Zhao, M.; Sun, L.; Chechik, V.; Yeung, L. K. *Acc. Chem. Res*. **2001**, *34*, 181−190.
(11) Scott, R. W. J.; Wilson, O. M.; Crooks, R. M. *J. Phys. Chem. B* **2005**, *109*, 692−704.
(12) Maiti, P. M.; Cagin, T.; Wang, G.; Goddard, W. A., III. *Macromolecules* **2004**, *37*, 6236−6254.
(13) Hendricks, R. W. *J. Appl. Crystallogr*. **1972**, *5*, 315−324.
(14) Bonse, U.; Hart, M. *Appl. Phys. Lett*. **1968**, *7*, 238−240.
(15) Koga, T.; Hart, M.; Hashimoto, T. *J. Appl. Crystallogr*. **1996**, *29*, 318−324.
(16) Nagaya, T.; Orihara, H.; Ishibashi, Y. *J. Phys. Soc. Jpn*. **1989**, *58*, 3600−3605.
(17) Nakai, A.; Shiwaku, T.; Wang, W.; Hasegawa, H.; Hashimoto, T. *Macromolecules* **1996**, *29*, 5990−6001.
(18) Percus, J. K.; Yevick, G. J. *Phys. Rev.* **1959**, *110*, 1−13.
(19) Sakamoto, N.; Harada, M.; Hashimoto, T., *Macromolecules* **2006**, 39, 1116−1124.
(20) *Dynamic Light Scattering*; Brown, W. Ed.; Clarendon Press: Oxford, 1993.
(21) In the case, when interdendrimer aggregates are formed, polymer effects concerning deformation of dendrimer conformations, which are induced by the interdendrimer cross-linkings as discussed here and by the growth of Pd nanoparticles as discussed in section 5.3. (in the beginning of page 4336) of ref 1, may become important in addition to the following polymer effects encountered when dendrimers are molecularly dispersed in the solution: detailed density profiles inside dendrimers and the relative location of nanoparticles inside the dendrimers.
(22) It should be noted that in Figure 5b there is a slight discrepancy between the theoretical and experimental scattering profiles at the high q region around $q = 0.2-0.3$ nm^{-1} as shown by the two arrows (especially so in the case of larger Z). The discrepancy can be seen in the broad scattering maximum in the experimental profiles #2 to #4, which arises from interference of the scattering field from the Pd nanoparticles inside the templates. The inter−nanoparticle interference may becomes significant when the number density of Pd nanoparticles inside the templates increases with increasing Z values (as evidenced from the increased ϕ_n value from 1 to 2.3 as shown in Table 4). In this case, $S_{nano}(q)$ could be better described by the Percus−Yevick (PY) type hard sphere model [18,19] rather than the independent sphere model employed in this work. However, the scattering analysis based upon the PY model was not conducted, as it is beyond the scope of the present work. Moreover, the value R_{nano} estimated in this work will not be hardly affected by the inter−nanoparticle interference, because the best fit was conducted on the profiles at $q > 0.3$ nm^{-1} where the interference effect becomes insignificant.
(23) The SANS intensity at a smallest q, I_s, tends to decrease with increasing Z. This tendency is explained in terms of the independent scattering model from the templates $I_s \propto N_{temp}R_{temp}^6$: The ratio for I_s for $Z = 21$ to I_s for $Z = 43$ directly evaluated from the experimental SANS profiles is equal to 2.05, while the ratio for $N_{temp}R_{temp}^6$ evaluated from N_{temp} and R_{temp} in Table 4 for $Z = 21$ and those for $Z = 43$ is equal to 1.95; the two values are in good agreement.
(24) Tanaka, H. Ph.D. dissertation, Graduate School of Engineering, Kyoto University, Kyoto, Japan 2008.
(25) Prosa, T. J.; Bauer, B. J.; Amis, E. J. *Macromolecules* **2001**, *34*, 4897−4906.
(26) Porod, G. *Kolloid-Z* **1951**, *124*, 83−114.

MA702034X